Light Metals 2014
Edited by: John Grandfield
TMS (The Minerals, Metals & Materials Society), 2014

CONTACTLESS ACOUSTIC WAVE GENERATION IN A MELT BY ELECTROMAGNETIC INDUCTION

Georgi Djambazov[1], Valdis Bojarevics[1], Bruno Lebon[1], Koulis Pericleous[1]
[1]The University of Greenwich, London SE10 9LS, UK

Keywords: Contactless Ultrasound, Cavitation, Induction Stirring

Abstract

Ultrasound treatment of molten metals is used for degassing, to refine microstructure, or disperse immersed particles. The process is most effective when vibrations lead to cavitation. A contactless method of generating sound waves is investigated using electromagnetic (EM) induction. Advantages over an immersed sonotrode would be lack of contamination in reactive melts, strong induced stirring due to Lorentz forces and application to high temperature materials. The induction coil surrounding the crucible - also used to melt the alloy - may be adopted for this purpose with suitable tuning. Numerical simulations of the sound generation have been performed for various cases, with and without resonance in the melt volume, with and without an auxiliary DC field. A computational acoustics approach is coupled with Maxwell's equations, and likely cavitation zones are identified using the Rayleigh-Plesset equation. Near-resonance conditions are most likely to produce cavitation without mechanically endangering the crucible.

Introduction

Vibration of the liquid metal during solidification is known to refine microstructure [1,2]. This can be accomplished using a mechanical stirrer inserted in the melt, or more commonly using an ultrasonic horn. The latter has been extensively used in the casting of aluminum ingots [2]. In ultrasonic processing, frequencies around 20 kHz are found to have the most effect, and this is attributed to the onset of cavitation. Gas micro-bubbles in the liquid (present either due to dissolved gases, or attached to particles), subjected to the imposed pressure sine wave first expand non linearly to many times their original size and then collapse violently generating high speed micro-jets which break up emerging dendrites or facilitate the dispersion of oxide particles generating nucleation sites. Evidence of cavitation has been found in post solidification analysis and it was further shown to depend on a critical pressure threshold [3]. Of relevance to the present study, within the ExoMet project [4], ultrasonic processing is one of the candidate techniques for the production of MMNCs.

There are however, several disadvantages in immersive stirring/vibration techniques: contact with the liquid metal leads to contamination of the melt and conversely erosion of the immersed surface, requiring frequent replacement. These problems are magnified when dealing with high temperature alloys (Steel, Nickel) or with highly reactive metals (Ti, Zr,…). Another disadvantage of the immersed sonotrode is the localized effect of the cavitation region. Vives [5], was the first to suggest a non-contact technique, using a combination of static and AC magnetic fields. Other investigators followed this lead, using different configurations for AlSi hypereutectic alloys [3], for grey iron melts [6] and aluminum alloys etc. In each case, different thresholds of pressure amplitude were found to be necessary and a range of frequencies was used, from 50 Hz to 50 kHz. There has been no systematic study of the sound field generated in these situations and this is the objective of this study.

Problem Setup

A typical ceramic induction crucible is shown in Fig. 1.

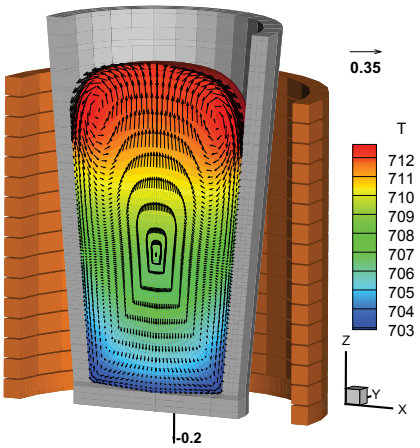

Fig. 1: Aluminum processing crucible surrounded by 2 kHz, 1.6 kA induction coil with computed velocity and temperature fields.

The Lorentz force generated by the induction coil acts in a thin layer of the metal, closest to the coil (Fig. 2) and it contains both time-averaged and time-dependent components. Fig. 1 shows the effect of the time-averaged force on the liquid metal, which induces strong stirring and deforms the free surface into a dome.

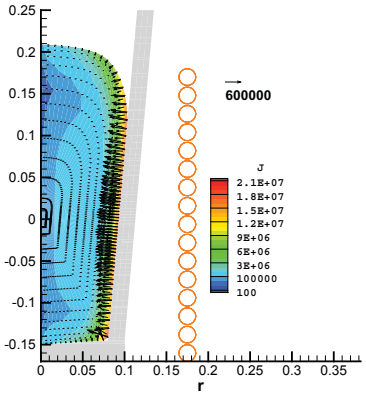

Fig. 2: Induced current and time-averaged Lorentz force

At the same time, the liquid metal is subjected to a periodic excitation by the AC magnetic field, which is responsible for the creation of sound waves. For the sound wave analysis, we will neglect the base and top surface effects in the crucible. In effect,

we are then dealing with a long cylindrical crucible filled with liquid metal and surrounded by an induction coil.
First, one-dimensional approximation along the radial direction ***x*** is assumed. The magnetic field vector (whose direction is ***z***) is parallel to the surface; the ***x***-coordinate runs from the surface inwards (-r) and the induced current is in the circumferential direction.

The Mathematical Model and Results

The parameters used in the calculations are given in Table 1.

Magnetic field amplitude	B_0	0.1	T
Frequency of excitation current	f_0	10000	Hz
Electrical conductivity	σ	4.1E+6	$\Omega^{-1}m^{-1}$
Density	ρ	2400	kg/m^3
Speed of sound in the liquid metal	c	1500	m/s
Spatial resolution factor	$n_\delta = \Delta x/\delta$	0.1	-
Temporal resolution factor	$CFL = c\Delta t/\Delta x$	0.995	-
Magnetic permeability	μ	$4\pi.10^{-7}$	$H\cdot m^{-1}$

Table 1: Problem Parameters

In aluminum, the characteristic length of the EM skin layer is $\delta = \sqrt{2/\mu\sigma\omega}$ = 2.48 mm where $\omega = 2\pi f_0$ is the angular frequency of the electromagnetic field. The analytical expression for the magnetic field is given as

$\boldsymbol{B} = B_R \cos\omega t + B_I \sin\omega t$ with

$B_R = B_0 e^{-\frac{x}{\delta}} \cos\frac{x}{\delta}$; $B_I = -B_0 e^{-\frac{x}{\delta}} \sin\frac{x}{\delta}$.

Consequently, the induced current $\boldsymbol{J} = J_R \cos\omega t + J_I \sin\omega t$ is defined by

$J_R = \sigma\frac{\omega}{2}\delta(B_R + B_I)$; $J_I = \sigma\frac{\omega}{2}\delta(B_I - B_R)$.

The electromagnetic Lorentz force in the metal is $\boldsymbol{F} = \boldsymbol{J} \times \boldsymbol{B}$ and its time-averaged value:

$\bar{F} = \frac{1}{2}(J_R B_R + J_I B_I) = \frac{1}{2\mu\delta} B_0^2 e^{-2\frac{x}{\delta}}$.

The time-averaged pressure created by this force in the liquid metal is

$p_S = \int_0^\infty \bar{F}(x)\,dx \approx \int_0^{7\delta} \bar{F}(x)dx = 1986$ Pa,

where the length of the computational domain 7δ was chosen sufficiently far from the skin layer for the above approximation to be valid. This corresponds to an 84mm metallostatic head (at the assumed B_0 = 0.1 T).

The time-dependent Lorentz force (under the 1D assumption) is

$$J.B = \frac{1}{2\mu\delta} B_0^2 e^{-2\frac{x}{\delta}} \left[1 + \sqrt{2}\cos\left(2\omega t - 2\frac{x}{\delta} + \frac{\pi}{4}\right)\right]$$

This formula shows that the mechanical excitation will have twice the frequency of the EM field. Figure 3 shows that force as a function of time at four different depths from the surface. It can be seen that a positive (pushing into the metal) steady component exists, i.e. $\bar{F}$, and that the amplitude decreases rapidly in the skin layer and it has almost vanished at $\frac{3}{2}\delta$ (see also Fig. 2). A phase shift is visible, increasing as the EM field penetrates below the surface.

The generation of sound waves by the alternating magnetic force was simulated using a Computational Acoustics approach. In one dimension, the equation of mass continuity and the simplified (no convection or viscous terms) momentum equations yield the following system:

$$\frac{\partial p}{\partial t} + \rho c^2 \frac{\partial \tilde{u}}{\partial x} = 0 \;\; ; \;\; \rho\frac{\partial \tilde{u}}{\partial t} + \frac{\partial p}{\partial x} = f \;, \; f = |\mathbf{F}| - \bar{F} \;.$$

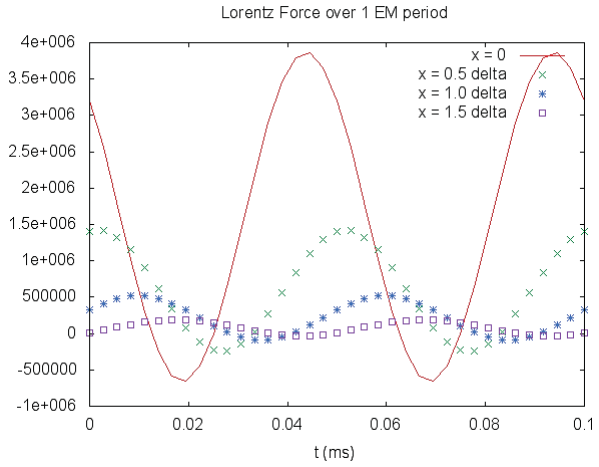

Fig. 3: EM force in the metal at four positions from the surface.

This system of 1st order partial differential equations was discretized onto a *fully-staggered* mesh [7] formed of the spatial axis x and the temporal axis t. The acoustic pressure values p were stored on the cell faces of this mesh and the acoustic velocity perturbations $\tilde{u}$ were in the cell centres in the middle of each time step – this leads to the 'leap frog' numerical scheme. The time-dependent component of the force f was evaluated in the 'u' positions and added to the right-hand side of the momentum equation.

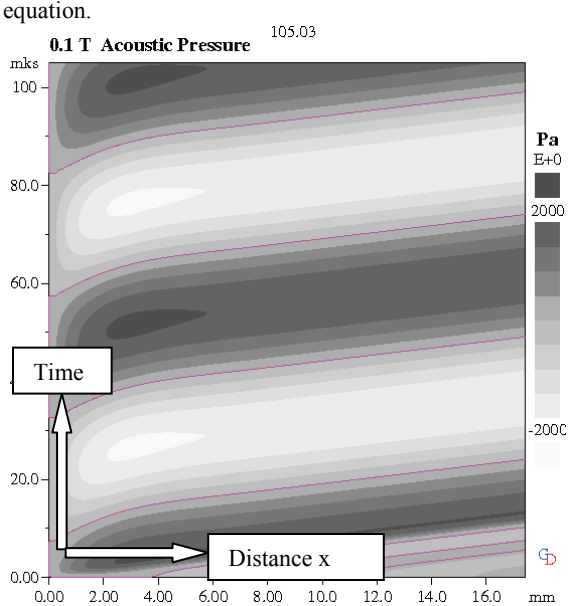

Fig. 4: Acoustic pressure variation at 0.1 T field amplitude.

The initial condition was 0 for all variables; the boundary condition on the surface was $p = 0$ and in the other end of the domain a simplified, approximate acoustic radiation boundary condition was applied which allows the sound waves to leave the

computational domain without false reflection at the boundary. (It should be noted that the 7δ domain is much shorter than the acoustic wavelength and no resonance studies were attempted with this set up). Mesh independence of the result was checked by making Δx two times smaller and 5 times smaller (and simultaneously adjusting Δt keeping the CFL number the same).

The result of the simulation is shown in Fig. 4, with contours of the calculated p as a function of x (horizontal) and t (vertical). It can be seen that the zone of sound generation extends about 2δ below the surface (x=0). The simulated time interval was just over one whole period of the EM excitation field; the resulting force and acoustic field have twice the frequency. The predicted acoustic amplitude for the given parameters is about 2000 Pa – this means a small vacuum of ~14 Pa will develop at the troughs of the passing waves. From previous studies, it is clear that the amplitude generated will be insufficient for cavitation. In that case resonance has to be created in a suitable configuration to achieve pressures in the negative phase which are sufficiently low (-1MPa) for cavitation.

Resonant Acoustic Pressure Evolution

To achieve a high enough amplitude, the diameter of the crucible was matched to the frequency of excitation by the relation $2R = c/f_1$, where R is the crucible radius and f_1 the first resonant frequency. The acoustic pressure is computed for two radii, with resonant frequencies equal to 2.5 kHz and 25.0 kHz respectively. The graphs in Figures 5 and 6 illustrate the evolution of the acoustic pressure along the axis of the crucible for the above cases and demonstrate that pressure levels compatible with cavitation are achievable. The next step is to compute the behavior of micro bubbles, placed in this field.

Dynamics of Spherical Bubbles

Assuming that bubbles are spherical, immersed in an incompressible Newtonian liquid, that processes occur so fast that they can be considered as adiabatic, and that bubbles are saturated with vapor whose partial pressure is the vapor pressure at the liquid bulk temperature, the Rayleigh-Plesset equation describes the evolution of the bubble radius with time:

$$\rho\left[R\ddot{R}+\frac{3}{2}\dot{R}^2\right]=p_v-p_\infty+p_{g_0}\left(\frac{R_0}{R}\right)^{3\gamma}-\frac{2S}{R}-4\mu\frac{\dot{R}}{R}$$

Where ρ is the density of the liquid, R is the radius of the bubble, p_v is vapour pressure, p_∞ is the pressure in the liquid, p_{g_0} is the initial gas bubble pressure, R_0 the initial bubble radius, S is the surface tension of the liquid-gas interface, and μ is the liquid viscosity. At time $t = 0$ s, the bubble is stable and the pressure in the liquid is given by

$$p_{\infty_0}=p_{g_0}+p_v-\frac{2S}{R_0}$$

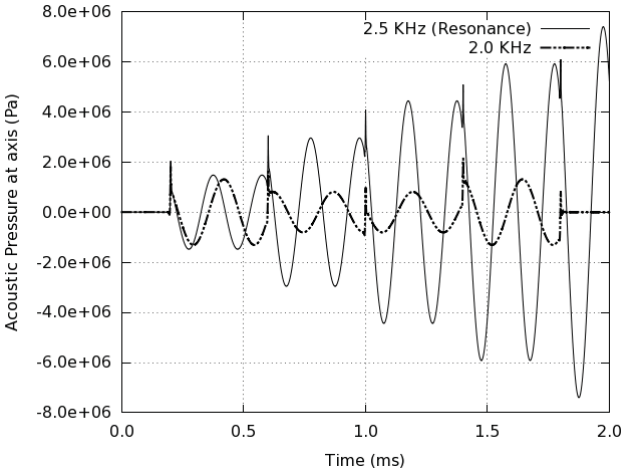

Fig. 5: Acoustic pressure variation for 2.5 kHz resonance.

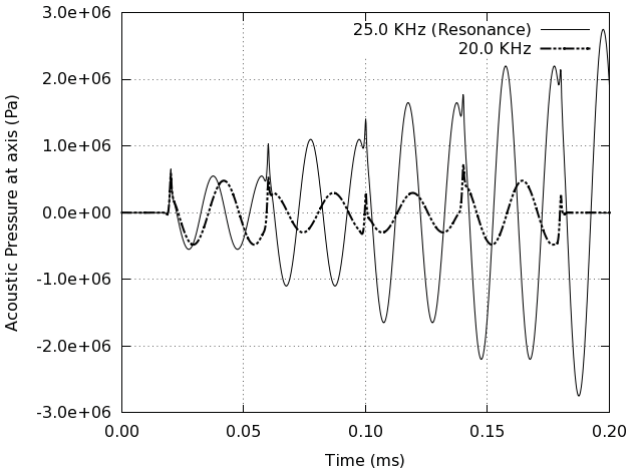

Fig. 6: Acoustic pressure variation for 25.0 kHz resonance.

The acoustic pressure variation given in Fig. 5 and Fig. 6 is applied to bubbles of hydrogen immersed in liquid aluminum for three different initial radii: 1 µm, 10 µm and 100 µm. Solving the Rayleigh-Plesset equation numerically (with a standard 4th order Runge-Kutta scheme) gives the results in Fig. 7 and Fig. 8.

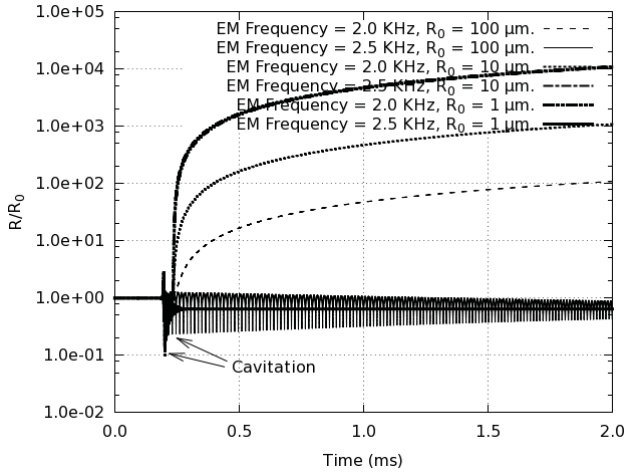

Fig. 7: Bubble radius evolution for cases run at 2.5 kHz. The ordinate is normalized with the initial bubble radius, and a log scale is used due to the large numerical difference in bubble evolution.

At lower frequencies (Fig. 7), cavitation (bubble collapse) occurs exclusively for the cases run with the resonant frequency 2.5 kHz. Irrespective of the initial size, all bubbles grow with an applied (B field) frequency of 2.0 kHz. At the resonant frequency, the bubbles all collapse as soon as the excitation field is applied.

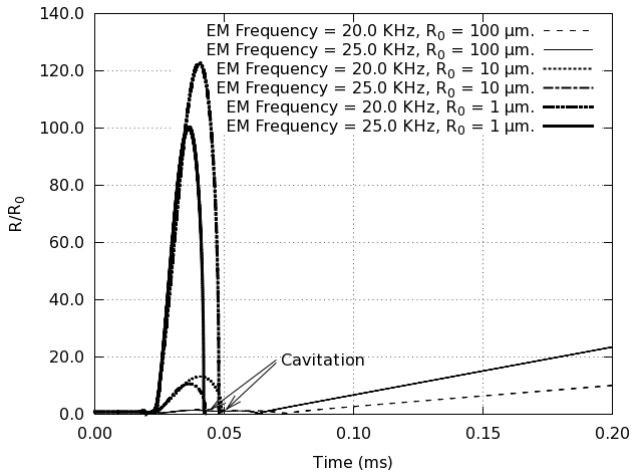

Fig. 8: Bubble radius evolution, for cases run at 25.0 kHz.

With the higher set of frequencies (Fig. 8), bubbles with initial radii 1 µm and 10 µm collapse; the collapse happens earlier at the resonant frequency of 25.0 kHz. The larger bubble (with initial radius 100 µm) grows, with growth being faster at the resonant frequency. The results, demonstrate that cavitation is possible in liquid aluminum, provided the externally applied EM force is amplified by resonance. In a real situation, the free surface and possibly the walls of the crucible will absorb some of this energy, but near-resonance conditions can still be effective as shown in Fig. 9, where the resonant frequency - in this case 3.125 kHz appropriate for the crucible in Fig. 1 – has been altered by +/- 10%. Periodic amplitudes exceeding 2 MPa are still achievable.

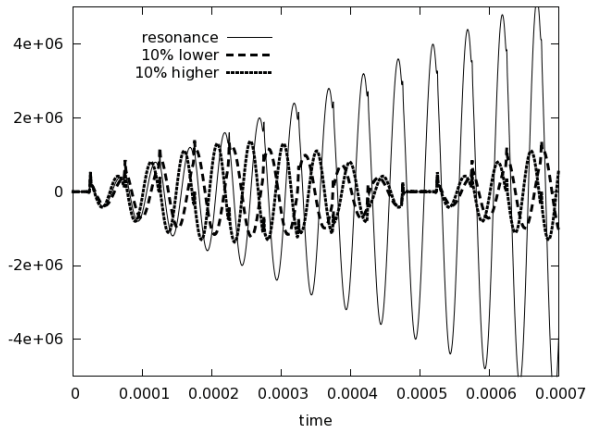

Fig. 9: Acoustic pressure variation at the axis, obtained at resonant and near-resonant force conditions.

Conclusions

In the search for a contactless "ultrasonic" cavitation device for liquid metal processing, this study computes the sound field generated in a crucible using external electromagnetic excitation. The induction coil used for melting the contents of the crucible, and for stirring, also provides the excitation. The sinusoidal part of the Lorentz force will decay quickly outside the skin layer and by itself is too weak to generate cavitation. Tuning the induction coil frequency to near cylindrical resonance conditions achieves the required goal. Cavitation level pressures are achieved over a large part of the melt volume, coupled with strong electromagnetic convection stirring. Experiments to validate these theoretical stipulations will be conducted in the near future.

References

1. O. Abramov, Ultrasound in Liquid and Solid Metals (Boca Raton, FL: CRC Press, 1994), p. 289
2. G.I. Eskin, D.G. Eskin, "Production of natural and synthesized aluminum-based composite materials with the aid of ultrasonic (cavitation) treatment of the melt", *Ultrasonics Sonochemistry*, Vol. 10, 4–5, (2003), p. 297
3. A. Radjai, K. Miwa, T. Nishio - *Metal and Mat Trans A*, 1998
4. ExoMet Project, European Commission contract FP7-NMP3-LA-2012-280421
5. C. Vives (1996) "Crystallization of aluminium alloys in the presence of cavitation phenomena induced by a vibrating electromagnetic pressure" *Journal of Crystal Growth* 158, pp.118-127
6. A. Radjai, K. Miwa, "Structural refinement of gray iron by electromagnetic vibrations", *Metall Mat Trans A*: Vol 33, 9, (2002), p. 3025
7. G.S. Djambazov, Numerical techniques for computational aeroacoustics., PhD thesis, University of Greenwich (1998)

Acknowledgments

The authors acknowledge financial support from the ExoMet Project (co-funded by the European Commission (contract FP7-NMP3-LA-2012-280421), by the European Space Agency and by the individual partner organizations)